24th Symposium on Naval Hydrodynamics
Fukuoka, JAPAN, 8-13 July 2002

Development, validation and application of a time domain seakeeping method for high speed craft with a ride control system.

F. van Walree (Maritime Research Institute Netherlands)

ABSTRACT

A computational method for the seakeeping behaviour of ships with a ride control system is described. The method essentially is a time domain panel method using the transient Green function to incorporate free surface effects. It is designed to take ship hulls with lifting surfaces into account.

Validation results are presented for three basic cases: damping forces on an oscillating lifting surface operating beneath a free surface, wave excitation forces on a lifting surface advancing in waves and wave induced motions of a destroyer hull form operating in head seas.

Next, application of the method to high speed craft with ride control is discussed and motion predictions are validated. Special attention is paid to interaction effects between a ship hull and a set of T-foil stabilizers.

Finally, linear and non-linear motion predictions for an unconventional frigate hull form are presented.

INTRODUCTION

The last decades have shown an increasing use of ride control systems for improving the manoeuvrability and comfortability of ships in a seaway. Control surface types include roll stabilisation fins, trim flaps, interceptors and T-foils. The use of such control surfaces is often limited by maximum deflection angles and rotational velocities, stall and, at high speed, by cavitation. These limitations restrict the applicability of frequency domain prediction methods for wave induced motions and loads, since these are based on the principle of a linear behaviour of all components present. Time domain methods are not necessarily based on the assumption of linearity and therefore provide a good basis for seakeeping calculation methods for ships equipped with a ride control system. Furthermore, besides the ability to include non-linear control surface characteristics, an additional advantage is that the mutual interaction between a control surface and the hull may be included in a straightforward manner.

The present paper describes the development and application of a time domain calculation method for the seakeeping behaviour of ships equipped with a ride control system. The motivation for this development originates from consultancy experiences at MARIN. An example of this experience is described in the following paragraphs.

During the design stage of a high speed mono hull the procedure followed to obtain the motion damping effect due to a set of T-foils was as follows. The lift forces acting on the T-foils in isolation were obtained by means of a lifting surface method, see Van Walree (1999). Next, the reduction in pitch motion of the mono hull was obtained by superimposing restoring and damping moments due the T-foil lift force in the equations of motion of a three-dimensional boundary element method based on a linear frequency domain theory. In this procedure the mutual interaction between the T-foils and the hull bottom was neglected. The reductions in vertical accelerations were in the order of 50%, that is a reduction by a factor two.

Subsequently, an extensive experimental program was carried out on the seakeeping characteristics of the craft with and without T-foils. The effect of the T-foils turned out to be much lower than anticipated: the accelerations were reduced by 15 to 25% only instead of the anticipated 50%.

At that time an investigation was started into the causes for this discrepancy. A possible cause, the loss of lift due to scale effects, was investigated and the effects were found to be small. Another cause for loss of lift was that the limitation on the T-foil incidence with respect to cavitation and stall considerations was often met during the experiments. Next, the configuration was analysed by means of a steady flow panel method usually applied to optimise hull forms with respect to wave making resistance. The results showed that the lifting efficiency of the T-foils could be

reduced by about 30% due to the interaction between the hull and T-foils.

It was therefore decided to develop a numerical method for wave induced motions which could take into account mutual interaction between the hull and control surfaces as well as non-linear control surface characteristics.

This paper addresses fundamentals and details of the numerical method as well as its validation for frigate and high speed craft types with and without ride control systems.

NUMERICAL METHOD

The numerical method is a combination and extension of the methods described by Lin and Yue (1990), Pinkster (1998) and Van Walree (1999). The problem is described in a space-fixed Cartesian co-ordinate system (x_0,y_0,z_0). The z_0-axis is pointing upwards and the x_0-y_0 plane is positioned in the undisturbed water surface. A body is considered that consists of one or more ship hulls in combination of one or more finite aspect ratio lifting surfaces of arbitrary planform. The body is considered to perform motions in six degrees of freedom.

The body is advancing through a homogenous and incompressible fluid. Surface tension is not included and the water depth is infinite. Incident waves from arbitrary directions are present. All vorticity in the flow is restricted to a thin region consisting of the outer skin of the lifting surface and its wake sheet. The flow outside this region is considered to be irrotational and inviscid.

The formulation of the problem is based on a mathematical formulation for large amplitude ship motions by Lin and Yue (1990). Their formulation is based on the use of impulsive sources to represent the unsteady flow about ship hulls only. The formulation described here includes also a combination of impulsive strength source and doublet elements representing a lifting surface.

A fluid domain $V(t)$ is considered, bounded by the free surface $S_F(t)$, the hull surface $S_H(t)$, the lifting surface $S_L(t)$, its wake sheet $S_W(t)$ and the surface at infinity $S_\infty(t)$. The normal vector is defined positive pointing in to the fluid domain. The motions in the fluid domain are described by a total velocity potential Φ:

$$\Phi(\underline{x}_0, t) = \Phi_d(\underline{x}_0, t) + \Phi_w(\underline{x}_0, t) \quad (1)$$

where $\underline{x}_0$ is the space-fixed position vector, t is time , Φ_d is the disturbance potential associated with the flow disturbances created by the body and Φ_w is the incident wave potential. The dependence of the potentials on $\underline{x}_0$ and t is dropped in the following for brevity. The incident wave potential is known a priori and can be shown to satisfy condition (4). The definition of the potential function for sinusoidal waves is:

$$\Phi_w = \frac{\zeta_a g}{\omega} e^{kz_0} \sin(k(x_0 \cos\psi + y_0 \sin\psi) - \omega t) \quad (2)$$

where ζ_a is the wave amplitude, ω is the wave frequency, ψ is the wave direction, k is the wave number ($k=\omega^2/g$) and g is the gravitational constant. The disturbance potential Φ_d satisfies the Laplace equation (for $t>0$):

$$\nabla^2 \Phi_d = 0 \quad (3)$$

On the undisturbed free surface $S_F(t)$, the following linearized condition is imposed (for $t>0$):

$$\frac{\partial^2 \Phi_d}{\partial t^2} + g \frac{\partial \Phi_d}{\partial z_0} = 0 \quad (4)$$

On the instantaneous body surface, consisting of hull surface $S_H(t)$ and lifting surface $S_L(t)$, the tangential flow condition is imposed (for $t>0$):

$$V_n = \frac{\partial \Phi_d}{\partial n} + \frac{\partial \Phi_w}{\partial n} \quad (5)$$

where V_n is the instantaneous normal velocity of the body. The $\partial/\partial n$ operator denotes the derivative in normal direction, $\partial/\partial n = n.\nabla$. The term $\partial\Phi_w/\partial n$ denotes the wave orbital velocity component normal to the body surface. The conditions at infinity (S_∞) are (for $t>0$):

$$\Phi_d \to 0 \text{ and } \frac{\partial \Phi_d}{\partial t} \to 0 \quad (6)$$

Apart from incoming waves, the fluid is at rest at the start of the process, the initial conditions on the free surface $S_F(t)$ are then (for $t=0$):

$$\Phi_d = \frac{\partial \Phi_d}{\partial t} = 0 \quad (7)$$

The transient Green's function is now introduced for a submerged source and doublet with an impulsive

strength:

$$G(p,t;q,\tau) = G^0 + G^f = \frac{1}{R} - \frac{1}{R_0} +$$

$$2\int_0^\infty [1-\cos(\sqrt{gk}\,(t-\tau))\,]e^{k(z_0+\zeta)}J_0(kr)\,dk, \qquad (8)$$

$$\text{for } p \neq q,\ t \geq \tau$$

where $p(x_0,y_0,z_0)$ and $q(\xi,\eta,\zeta)$ are the field and singularity point co-ordinates respectively, τ is a past time variable, G^0 contains the source, doublet and biplane image parts and G^f is the free surface memory integral, J_0 is the Bessel function of order zero and

$$R = \sqrt{(x_0-\xi)^2 + (y_0-\eta)^2 + (z_0-\zeta)^2}$$

$$R_0 = \sqrt{(x_0-\xi)^2 + (y_0-\eta)^2 + (z_0+\zeta)^2} \qquad (9)$$

$$r = \sqrt{(x_0-\xi)^2 + (y_0-\eta)^2}$$

It can be shown that the Green's function, eq. (8) satisfies the following conditions, where $V(t)$ is the fluid domain:

$$\nabla^2 G = 0 \text{ in } V(t),\ t > \tau$$

$$\frac{\partial^2 G}{\partial t^2} + g\frac{\partial G}{\partial z_0} = 0 \text{ on } S_F(t),\ t > \tau$$

$$\text{G}, \frac{\partial G}{\partial t} \to 0 \text{ on } S_\infty, t > \tau \qquad (10)$$

$$\text{G}, \frac{\partial G}{\partial t} = 0 \text{ on } S_F(t),\ t = \tau$$

A boundary integral formulation for the problem is derived according to Pinkster (1998). The following equation results for the potential at field point p, located on $S_{HLW}(t)$:

$$4\pi\Phi_d(p,t) =$$

$$\iint_{S_{HL}(t)} \sigma(q,t)\,G^0\,dS + \iint_{S_{LW}(t)} \mu(q,t)\frac{\partial G^0}{\partial n_q}\,dS -$$

$$\int_0^t d\tau \iint_{S_{HL}(\tau)} \sigma(q,\tau)\frac{\partial G^f}{\partial \tau}\,dS + \int_0^t d\tau \iint_{S_{LW}(\tau)} \mu(q,\tau)\frac{\partial^2 G^f}{\partial \tau \partial n_q}\,dS +$$

$$\frac{1}{g}\int_0^t d\tau \int_{L_{w(\tau)}} \sigma(q,t)\frac{\partial G^f}{\partial \tau} V_N\,V_n\,dL \qquad (11)$$

where $\sigma(q,t)$ and $\mu(q,t)$ are the source and doublet strengths at position q, at time t, and $\partial/\partial n_q$ is the normal derivative at the singularity point q. V_n is the normal velocity on a waterline panel and is related to V_N by $V_N = V_n(\underline{N}.\underline{n})$. By applying the $\nabla.\underline{n}_p$ operator to eq. (11) and by using the tangential flow condition (5) on the hull and lifting surfaces $S_H(t)$ and $S_L(t)$ respectively, the following formulation is obtained:

$$4\pi\left(V_{np} - \frac{\partial \Phi_w}{\partial n_p}\right) =$$

$$\iint_{S_{HL}(t)} \sigma(q,t)\frac{\partial G^0}{\partial n_q}\,dS + \iint_{S_{LW}(t)} \mu(q,t)\frac{\partial^2 G^0}{\partial n_p \partial n_q}\,dS +$$

$$\int_0^t d\tau \iint_{S_{HL}(\tau)} \sigma(q,\tau)\frac{\partial^2 G^f}{\partial t \partial n_q}\,dS - \int_0^t d\tau \iint_{S_{LW}(\tau)} \mu(q,\tau)\frac{\partial^3 G^f}{\partial t \partial n_p \partial n_q}\,dS -$$

$$\int_0^t d\tau \int_{L_w(\tau)} \sigma(q,t)\frac{\partial^2 G^f}{\partial t \partial n_p} V_N\,V_n\,dL \qquad (12)$$

where $\partial/\partial n_p$ is the normal derivative at field point p and $\partial G/\partial\tau$ has been replaced by $-\partial G/\partial t$. Equation (12) is the principal equation to be solved for the unknown source and doublet strengths $\sigma(q,t)$ and $\mu(q,t)$ respectively. For lifting surfaces, it does not have an unique solution for the conditions implied so far. A wake model needs to be established where conditions are specified which relate to the vortex strength at the trailing edge and the location and shape of the wake sheet.

Wake model

The Kutta condition for steady and unsteady flow is that the velocity along the trailing edge of lifting surfaces remains finite. An additional condition is that vorticity must be shed from the lifting surface to the wake sheet in order to satisfy the requirement that in a potential flow the circulation Γ around a contour enclosing the lifting surface and its wake must be conserved. By using doublet elements on the lifting surface and (equivalent) vortex ring elements on the wake sheet with strength Γ as a discretization of a continuous vortex sheet and by transferring each time step the nett circulation at the trailing edge elements into the wake elements, these requirements are satisfied. Once shed, the circulation strength of wake sheet elements remains constant. Furthermore, the wake sheet should be force free as it is not a solid surface; no pressure difference must be present between the upper and lower sides of the sheet. For a force free wake sheet the vorticity vector should be directed parallel to the velocity vector. This can be accomplished by displacing the vortex element corner points with the local fluid velocity.

Discretization

On the ship hull constant strength, quadrilateral source panels are used. On the lifting surface a combination of constant strength, quadrilateral source and doublet panels are used. The source strength of lifting surface panels is predefined, it equals the local normal velocity of the body minus the normal velocity due to incident waves. The doublet strength is determined from the tangential flow condition which is applied at the collocation point on each panel. On the wake sheets, vortex ring elements carrying a circulation strength Γ are used.

Time stepping process

At the start of the simulation (t=0) the body is impulsively set into motion. At this instant, the source and doublet strengths on the hull and lifting surface are determined for the condition without wake vortex elements. At each subsequent time step, the body is advanced to a new position with its instantaneous velocity. Both the position and velocity are known from the equations of motion. In the equations of motion, the accelerations are obtained from the forces acting on the body and the body inertia properties and are subsequently integrated in time yielding velocities and positions. The gap between the instantaneous trailing edge doublet panels on the lifting surface and the wake vortex element shed in the previous time step is filled with a new wake vortex element. In this way, the wake vortex element at the trailing edge has the same orientation as the flow leaving the trailing edge, to a first order approximation.

The circulation strength of new wake vortex elements created directly behind the trailing edge of the lifting surface is set equal to the difference in doublet strengths at the upper and lower side of trailing edge panels. The nett circulation strength is then zero, fulfilling the finite speed requirement at the trailing edge. With a known wake vortex position and circulation, hull and lifting surface position and velocity, the tangential flow condition, eq. (12) can be solved for the unknown source and doublet strengths.

Solution of the integral equation

For hull panels on $S_H(t)$ and doublet panels on $S_L(t)$, the discretized form of the integral eq. (12) is given by:

$$
\begin{aligned}
&\sum_{j=1}^{NH(t)} \sigma_j^{(t)} \iint_{S_j} \frac{\partial G^0(p_i,q_j)}{\partial n_{p_i}}\, dS + \\
&\sum_{j=1}^{NL(t)} \mu_j^{(t)} \iint_{S_j} \frac{\partial^2 G^0(p_i,q_j)}{\partial n_{p_i}\partial n_{q_j}}\, dS = \\
&-4\pi \underline{V}(p_i,t)\cdot \underline{n}_{p_i} - \\
&\sum_{j=1}^{NW(t)} \mu_j^{(t)} \iint_{S_j} \frac{\partial^2 G^0(p_i,q_j)}{\partial n_{p_i}\partial n_{q_j}}\, dS - \\
&\sum_{j=1}^{NL(t)} \sigma_j^{(t)} \iint_{S_j} \frac{\partial G^0(p_i,q_j)}{\partial n_{p_i}\partial n_{q_j}}\, dS - \\
&\int_0^t d\tau \sum_{j=1}^{NH(\tau)+NL(\tau)} \sigma_j^{(\tau)} \iint_{S_j} \frac{\partial^2 G^f(p_i,t;q_j,\tau)}{\partial t\partial n_{p_i}}\, dS + \\
&\int_0^t d\tau \sum_{j=1}^{NWL(\tau)} \sigma_j^{(\tau)} \int_{L_{wj}} \frac{\partial^2 G^f(p_i,t;q_j,\tau)}{\partial t\partial n_{p_i}} V_N^{(\tau)} V_n^{(\tau)}\, dL + \\
&\int_0^t d\tau \sum_{j=1}^{NL(\tau)+NW(\tau)} \mu_j^{(\tau)} \iint_{S_j} \frac{\partial^3 G^f(p_i,t;q_j,\tau)}{\partial t\partial n_{p_i}\partial n_{q_j}}\, dS
\end{aligned}
\qquad (13)
$$

where NH is the number of source panels on the hull surface, NWL is the number of waterline panels on the hull, NL is the number of doublet panels on lifting surfaces and NW is the number of wake elements, t is the present time, τ is the past time, i and j are the element indices for collocation point p and singularity point q respectively, $\partial/\partial n_{pi}$ denotes the normal derivative to the surface at collocation point i, $\partial/\partial n_{qj}$

denotes the normal derivative to the surface at singularity point j. Both normals are defined in the space-fixed axis system.

The terms on the left hand side in eq. (13) denote the normal induced velocity due to the source and doublet elements on the body and lifting surface respectively. The first term on the right hand side denotes the normal velocity components due to body motions and incident waves, the second and third terms denote the normal induced velocity due to wake vortex elements and lifting surface doublet panels, the fourth and fifth terms account for the normal induced velocity components due to the memory effect of hull and lifting surface source panels, the sixth term accounts for the normal induced velocity components due to the memory effect of waterline source panels and the last term on the right hand side accounts for the normal induced velocity due to the memory effect of lifting surface and wake sheet doublet panels.

The vector $\underline{V}$ denotes the velocity components due to the body translational velocities, $\underline{V}_b = (u,v,w)$ and angular velocities, $\underline{\Omega}_b = (p,q,r)$, and the orbital ($\underline{V}_w$) velocity components due to incident waves:

$$\underline{V}(p_i,t) = \underline{V}_b(t) + \underline{\Omega}_b(t) \times \underline{r}(p_i) - \underline{V}_w(p_i,t) \qquad (14)$$

Here $\underline{r}$ denotes the position vector of the field point p and all velocity components are defined in the space-fixed axis system. Eq. (13) can be cast in a set of linear equations in the unknown source and doublet strengths $X_j^{(t)}$:

$$\sum_{j=1}^{NT(t)} A_{ij}^{(t)} X_j^{(t)} = B_i^{(t)} \qquad i = 1,2,\ldots, NT(t) \qquad (15)$$

where A_{ij} contains the integral term of the left hand side of eq. (13) and B_i contains the entire right hand side of eq. (13). $NT(t)$ denotes the total number of source and doublet panels. This set of equations is solved by using common linear algebra techniques.

Linearization

The evaluation of a G^f term by direct numerical integration requires an impractical large amount of computer time. These terms must be evaluated at each control point for the entire time history of all singularity elements. An efficient evaluation of the G^f terms is therefore of importance. For low and moderate time values use is made of interpolation on a table of predetermined values for G^f and its derivatives, see Pieters (1999). For large time values is made of asymptotic expansions provided by Newman (1985,1992). Despite the efficient evaluation of the G^f terms, the required computer time is still substantial due to the required numerical integration both in time and in space. A more efficient evaluation of the G^f terms based on a combination of analytical and numerical evaluation is in development.

As a first step towards reduction of computer time and memory, the number of wake elements is set to a maximum. Once this maximum number is reached, new row of wake elements are still generated at the trailing edge, but the last row of wake elements (at maximum distance from the lifting surface) is removed. The maximum number of wake elements is set such that the wake has a sufficient length so that the effect of removing a row of wake elements on the body forces is negligible, see Van Walree (1999).

Next, the wake sheet position and form are prescribed. The prescription of the wake sheet position is simply that a wake sheet element remains stationary, once it is shed. This saves the determination of the actual position of the wake element corner points at each time step, for which the calculation of induced velocities at each wake element corner point due to all singularity elements is required. A prescribed wake sheet position violates the requirement of a force free wake sheet, but experience has shown that this has little effect on the forces acting on the lifting surfaces for practical conditions.

Still, for unsteady conditions, the wake sheet is not a flat surface behind the lifting surface. Since the lifting surface, shedding the wake vortex elements, performs arbitrary motions, the position of the wake sheet relative to the lifting surface varies and the induced velocities due all wake elements at the lifting surface have to be determined again each time step. For the panels on the hull and lifting surface a similar problem is present: the relative position between body panels and past time panels is not constant and the convolution integrals have to be completely computed each time step. The *non-linear* approach described so far requires the use of a powerful supercomputer.

However, the computer time can be significantly reduced for seakeeping problems for which the speed and heading are assumed constant and if the motions of the craft are assumed to be small. In eq. (13) the displacements of the craft around its mean position are not taken into account then. This will be termed the *linear* approach in the following.

The main advantage of linear simulations is that due to the constant relative distance between panels p_i and q_j, the convolution integrals may be computed only

once a priori for use at each time step in the simulation. The principle of influence coefficients is then used. Furthermore, a constant submerged geometry implies that the number of singularity elements on the body is constant. The influence coefficient matrix A in eq. (15) is then constant and needs to be inverted only once instead of each time step.

Prescribing the wake sheet shape in the linear approach results in a flat wake sheet in the x_0-y_0 plane behind the lifting surface. Due to the constant speed, the relative position between a row of wake elements and the lifting surface elements is constant. The concept of influence coefficients is again used, for determining the induced velocities due to wake sheet elements at the lifting surface collocation points. Furthermore, the integration of the $\partial G^f/\partial t$ terms with respect to time can be performed analytically for wake sheet vortex elements since the distance between body collocation points and wake elements is constant for each (t-τ) value, and the circulation of each wake element is constant in time.

Coupling steady and unsteady potentials for linear case

For linear (constant underwater geometry) simulations the so-called m-terms can be used to correct the boundary condition for the fact that it does not represent the instantaneous submerged body. The m-terms represent the velocity components at collocation points due to unit body displacements, for the steady condition. They are given by:

$$\begin{aligned}(m_1, m_2, m_3) &= -(\underline{n}\cdot\nabla)\ \underline{V} \\ (m_4, m_5, m_6) &= -(\underline{n}\cdot\nabla)\ (\underline{r}\times\underline{V})\end{aligned} \tag{16}$$

where $\underline{n}$ is the normal vector, $\underline{V}$ is the steady velocity vector and $\underline{r}$ is the position vector of collocation points. These terms are obtained from analytical differentiation of the free surface Green function G^f and the G^0 terms with respect to x, y, and z. The discontinuity in the derivative normal to a source panel is removed by using the fact that this normal derivative equals the w-velocity component of a doublet panel which is continuous at the doublet panel.

The m-terms are applied as follows in the tangential flow condition:

$$V_n = \underline{n}\cdot\dot{\underline{x}}_0 + \underline{m}\cdot\underline{x}_0 = \frac{\partial\Phi_d}{\partial n} + \frac{\partial\Phi_w}{\partial n} \tag{17}$$

It should be noted that the contribution to the components m_5 and m_6 due to the undisturbed flow Un_z and $-Un_y$ respectively, are already incorporated in the normal velocity components when body-fixed velocity components are transferred in to space-fixed velocity components. This is the case for the present method where the equations of motion are solved in a body-fixed axis system.

Force evaluation

The forces acting on the body are obtained from integrating the pressure over the panels. The pressure follows from the unsteady flow Bernoulli equation, in a body-fixed axis system, see Katz and Plotkin (1991):

$$\frac{p_{ref} - p}{\rho} = \frac{1}{2}\left\{\left(\frac{\partial\Phi}{\partial x}\right)^2 + \left(\frac{\partial\Phi}{\partial y}\right)^2 + \left(\frac{\partial\Phi}{\partial z}\right)^2\right\} + \frac{\partial\Phi}{\partial t} - (\underline{V} + \underline{\Omega}\times\underline{r})\cdot\nabla\Phi \tag{18}$$

where p denotes the pressure in the fluid, p_{ref} is a reference pressure, and Φ is the total velocity potential. $\underline{V}$ is the total velocity vector at the collocation point, due to the velocity of the body and the disturbance and wave orbital motion components.

For doublet panels on lifting surfaces the time derivative of the potential is obtained from a first order backward difference scheme:

$$\frac{\partial\Phi}{\partial t} = \frac{\partial\mu}{\partial t} \approx \frac{\mu(t) - \mu(t - \Delta t)}{\Delta t} \tag{19}$$

Using the same approach for the potential for source panels often yields instable results. Therefore a more accurate approach is taken as follows. The total potential is split into the disturbance potential and the incident wave potential. The time derivative of the latter potential can be computed analytically at each collocation point.

$$\begin{aligned}\frac{\partial\Phi}{\partial t} &= \frac{\partial\Phi_d}{\partial t} + \frac{\partial\Phi_w}{\partial t} \\ \frac{\partial\Phi_w}{\partial t} &= \frac{\partial}{\partial t}\left(\frac{\zeta_{wa} g}{\omega} e^{k_w z_0} \sin(k_w x_r - \omega t)\right)\end{aligned} \tag{20}$$

The time derivative of the disturbance potential Φ_d is split into two contributions (for source panels only) as follows:

$$4\pi\frac{\partial\Phi_d^0(p,t)}{\partial t}=\iint_{S_{HL}(t)}\frac{\partial\sigma(q,t)}{\partial t}G^0\,dS$$

$$4\pi\frac{\partial\Phi_d^f(p,t)}{\partial t}=\int_0^t d\tau\iint_{S_{HL}(\tau)}\sigma(q,\tau)\frac{\partial^2 G^f}{\partial t^2}\,dS-\frac{1}{g}\int_0^t d\tau\int_{L_w(\tau)}\sigma(q,\tau)\frac{\partial^2 G^f}{\partial t^2}V_N V_n\,dL \tag{21}$$

The time derivative of G^0 itself is zero, according to its definition. The terms on the right hand side of Φ_d^f are time derivatives of the memory integral and can be evaluated in a similar way as the free surface Green function terms. Furthermore, relations between the source strength and the corresponding potential and the source strength and the normal velocity component are used to obtain a relation for the Φ^0 contribution:

$$\begin{aligned}&\underline{\Phi}^0=C\cdot\underline{\sigma}\\&\frac{\partial\underline{\Phi}^0}{\partial t}=C\cdot\frac{\partial\underline{\sigma}}{\partial t}\\&\underline{\sigma}=A^{-1}\underline{v}_n\end{aligned} \tag{22}$$

to arrive at:

$$\frac{\partial\underline{\Phi}^0}{\partial t}=C\cdot A^{-1}\frac{\partial v_n}{\partial t} \tag{23}$$

where C is the influence coefficient matrix relating σ to Φ^0 and A^{-1} is the inverse of the normal velocity influence coefficient matrix from eq. (15).

The time derivative of the normal velocity $\underline{V}_n$ contains the following contributions:

$$\begin{aligned}&\frac{\partial\underline{V}_n}{\partial t}=\left[\frac{\partial\underline{v}_b}{\partial t}+\frac{\partial\underline{v}_G}{\partial t}-\frac{\partial\underline{v}_w}{\partial t}\right]\cdot\underline{n}\\&\frac{\partial\underline{v}_b}{\partial t}=\ddot{\underline{x}}_0+\ddot{\underline{\Omega}}\times\underline{r}\\&\frac{\partial\underline{v}_G}{\partial t}=\frac{\partial(\nabla\Phi_d^f)}{\partial t}\\&\frac{\partial\underline{v}_w}{\partial t}=\frac{\partial(\nabla\Phi_w)}{\partial t}\end{aligned} \tag{24}$$

The first contribution consists of the body acceleration components, these contributions can be transferred into an added mass matrix, in analogy with the added mass at infinite frequency used in frequency domain methods. The second contribution consists of the time derivative of the free surface Green function acceleration components which can be obtained from the time derivative of eq. (11). The third contribution consists of the wave orbital acceleration components which are obtained analytically from the wave potential.

Ventilated transom sterns

For ships with a transom stern it is assumed that the speed is sufficiently high so that the transom is fully ventilated, i.e. the flow smoothly separates at the transom edge. Methods using the transient Green function to account for free surface effects can not deal with such a flow. In order to compensate for this inadequacy two measures are taken. First, for craft with a relatively deep transom a dummy hull segment is positioned behind the transom. The dummy segment prevents the occurrence of unrealistically high tangential velocities (and accompanying suction forces) around the transom when the craft is heaving and pitching. The forces acting on the dummy segment itself are not taken into account. Second, the hydrodynamic pressure at the panel strip in front of the transom edge is set equal to the negative local hydrostatic pressure so that the total pressure equals the atmospheric pressure. By assuming a two-dimensional flow the longitudinal and vertical velocity components and the source strength at this last strip are corrected accordingly.

Viscous damping forces

High speed, slender hull forms usually have relatively little wave generation and an accompanying low potential flow damping. At the peak motion frequency viscous damping forces acting in the vertical plane may then be of importance. Viscous damping forces originate due to flow separation at the bilge region. The magnitude of these forces depends on the frequency of oscillation, Froude number and section shape. In the present computational method a cross flow model is used to account for viscous damping forces. The viscous drag coefficient depends on the section shape only, Froude number and frequency dependence is neglected. The following formulation is used in a strip wise manner:

$$F_z=-\frac{1}{2}\rho|V_r|V_r SC_D \tag{25}$$

where V_r is the vertical velocity of the section relative

to the local flow velocity and S is the horizontal projection of the section area. The cross flow drag coefficient C_D has a value in-between 0.25 and 0.80.

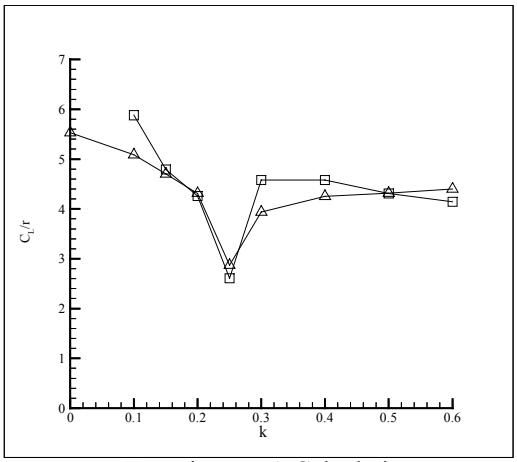
VALIDATION AND APPLICATION

In this section a number of validation and application cases will be discussed. The present version of the method can only deal with head and following wave conditions since no viscous damping forces for roll are included yet. Unless mentioned otherwise, all results have been obtained by using the linearized method. Ship hulls have been panelized according to their mean position at speed. This position was determined through a number (2-3) of runs at calm water with appropriate repanelization in between the runs. No m-terms are included other than these due to the undisturbed flow. It has been found that including the full m-terms (i.e. including the disturbed flow potentials) most times has an unfavorable effect on the predicted motions.

Lifting surface below free surface

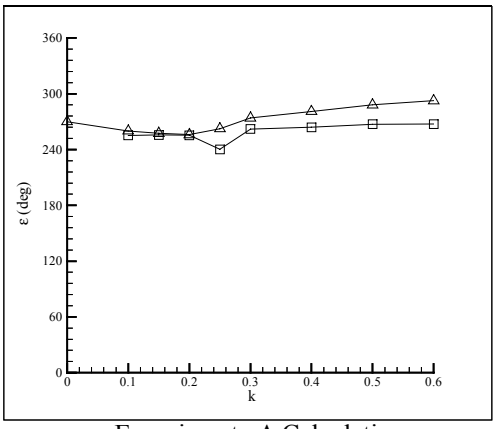
As a first validation case a comparison is made between experimental and computed results for the lift of an oscillating hydrofoil below the free surface. Experimental results are obtained from Kyozuka (1992). The experiments were conducted in a circulating water tunnel with a free surface. A rectangular lifting surface with a NACA-0012 section and aspect ratio AR=4.5 was oscillated in a direction normal to the chord line (heave) at a constant free stream velocity (F_{nc} =0.71). The oscillation amplitude z_a was 10% of the chord. The mean submergence to chord ratio was h/c=0.9. The centre section of the lifting surface (55% of the span) was mounted in between two dummy span parts. The loads were measured on the centre section only so that results for a two-dimensional flow were approximated. In the computations the forces acting on the appropriate part of the span were taken. Figures 1 and 2 show the normalised force amplitude, C_L/r, r=$\omega z_a/U$, and its phase angle ε with respect to the oscillatory motion.

The variation in force amplitude with reduced frequency k=$\omega c/2U$ is well predicted. U is the flow speed, c is the foil chord and ω is the frequency of oscillation. The dip in force amplitude at k=0.25 is due to wave making effects. This reduced frequency corresponds to the non-dimensional frequency τ_ω=$\omega U/g$=0.25. A shift in phase relative to ε=270 deg. also appears at this frequency. The phase angle is well predicted at low reduced frequencies but deviates somewhat at higher reduced frequencies.



□ Experiment Δ Calculation

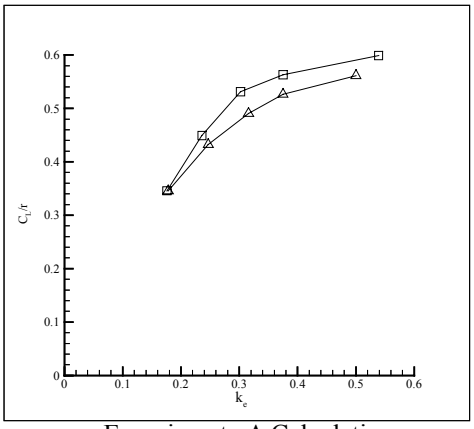
Fig. 1 Normalized lift amplitude on an oscillating hydrofoil below the free surface.



□ Experiment Δ Calculation

Fig. 2 Phase of lift wrt. oscillatory motion for a hydrofoil below the free surface.

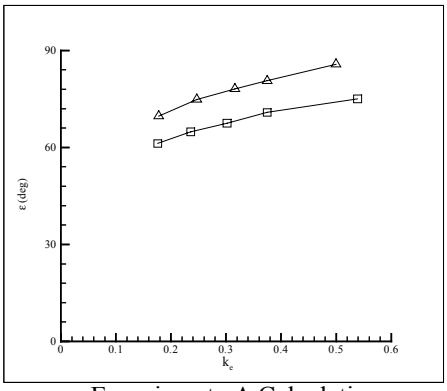
Figure 3 shows experimental and calculated wave induced forces on a lifting surface versus the reduced frequency k_e, based on the frequency of encounter. The experimental data are obtained from Wilson (1983). The foil has an aspect ratio of six, a submergence of half a chord, h/c=0.50, and advances in head waves. The foil has a NACA 64A010 symmetrical section. The regular waves have an amplitude of approximately 0.22 foil chords. The normalised amplitude for the lift force based on the wave amplitude and chord length, C_L/r, r=$2\zeta_a/c$, is well predicted.



□ Experiment Δ Calculation

Fig. 3 Normalized lift amplitude on a hydrofoil advancing in waves.

Figure 4 shows that the increase of the phase lead between the lift force and the wave elevation is also well predicted, however its magnitude deviates somewhat from the experimental values.

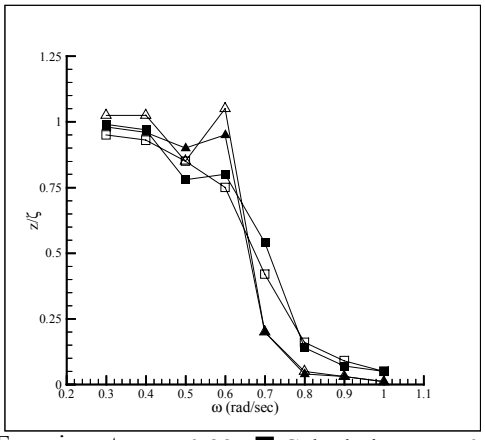


□ Experiment Δ Calculation

Fig. 4 Phase of lift wrt. wave elevation for a hydrofoil below the free surface.

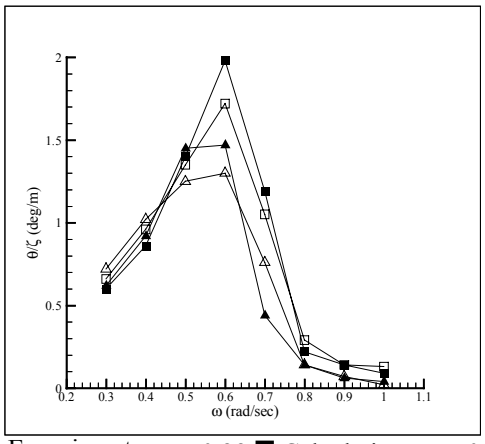
Destroyer

As a first validation case for a ship, experimental and computed heave and pitch motions of a 140 m destroyer (DDG51) sailing in regular head waves at two speeds (F_{nL}=0.23 and 0.39) are compared in Figures 5 and 6. Both the heave and pitch are well predicted at both speeds, although the peak pitch response is somewhat overpredicted for the highest speed.



□ Experiment, F_{nL} =0.23 ■ Calculation F_{nL} =0.23
Δ Experiment, F_{nL} =0.39 ▲Calculation F_{nL} =0.39

Fig. 5 Heave response of DDG51destroyer in head waves.



□ Experiment, F_{nL} =0.23 ■ Calculation F_{nL} =0.23
Δ Experiment, F_{nL} =0.39 ▲Calculation F_{nL} =0.39

Fig. 6 Pitch response of DDG51destroyer in head waves.

High speed mono hull ferry

The next case concerns a high speed (F_{nL}=0.67) mono hull ferry with a waterline length of about 100 m (TMV114). This craft is equipped with forward and aft T-foils with active incidence control. Figure 7 shows the panelization on the below water portion of the craft, including the dummy part behind the transom stern. Before discussing motion responses with and without T-foils, first the effect of modeling the transom stern flow is shown.

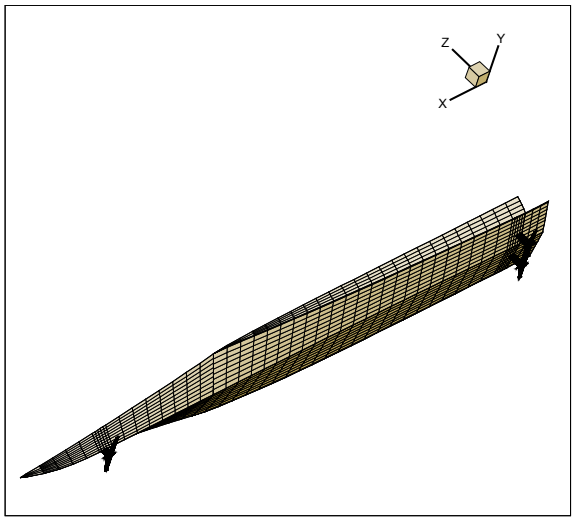
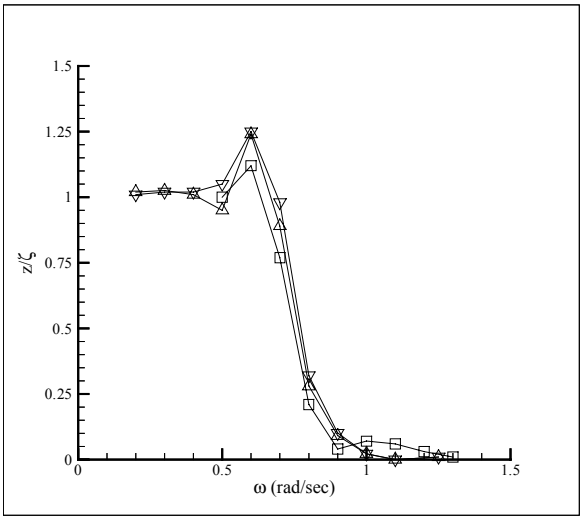


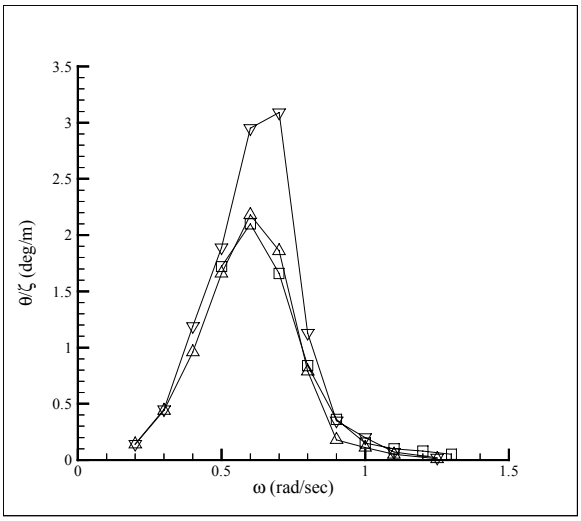
Fig. 7 Paneling arrangement on fast mono hull TMV114.

Figures 8 and 9 show the heave and pitch response in head waves, without T-foils. It is seen that without transom stern flow model the peak pitch response is significantly overestimated. The effect on the heave motion is small. The predicted responses are seen to be close to the experimentally obtained response functions (both in regular waves). Although not shown here, phase angles of heave and pitch with respect to the wave elevation have been found to be in good agreement with the experimental data as well.



□ Experiment
Δ Calculation with transom stern model
∇ Calculation without transom stern model

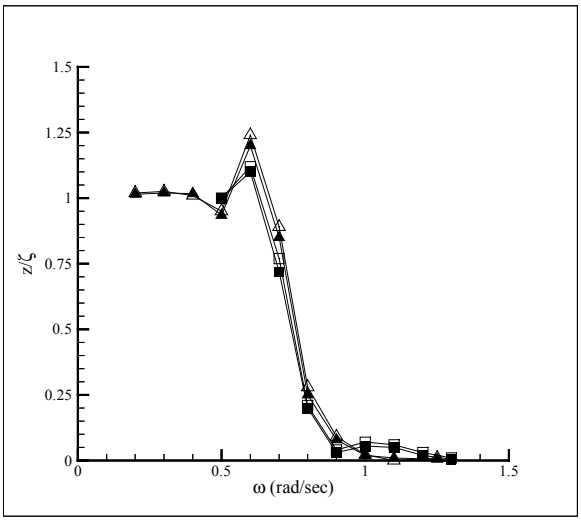
Fig. 8 Heave response of TMV114 in head waves at F_{nL} =0.57.



□ Experiment
Δ Calculation with transom stern model
∇ Calculation without transom stern model

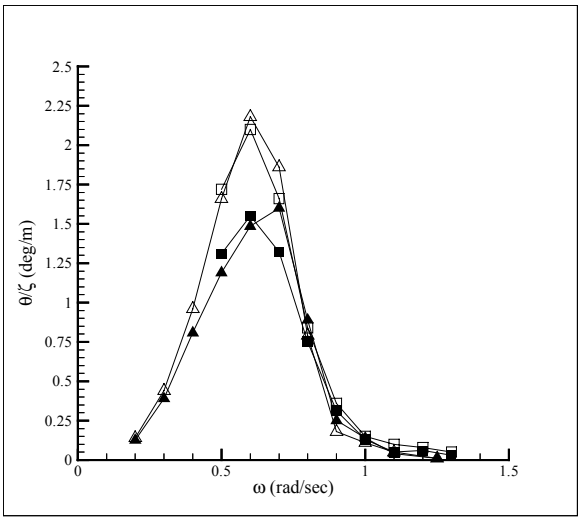
Fig. 9 Pitch response of TMV114 in head waves at F_{nL} =0.57.

Figures 10 and 11 show a comparison between the heave and pitch response in head waves with and without T-foils.



□ Experiment without foils
■ Experiment with active foils
Δ Calculation without foils
▲ Calculation with active foils

Fig. 10 Heave response of TMV114 in head waves at F_{nL} =0.57.



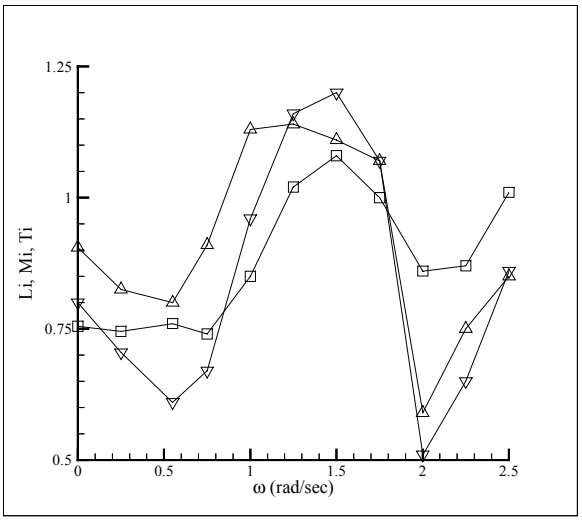
□ Experiment without foils
■ Experiment with active foils
Δ Calculation without foils
▲ Calculation with active foils

Fig. 11 Pitch response of TMV114 in head waves at F_{nL} =0.57.

It is seen that the effect of the T-foils is correctly predicted although the peak response differs somewhat. The reduction in motions is however relatively small and as stated in the introduction, much smaller than anticipated beforehand. The reasons for this are as follows:

- The foils were designed to operate at a speed at and above $F_{nL} = 0.67$, while the maximum experimental speed corresponded to $F_{nL} = 0.57$. This speed difference results in a loss of foil lift of almost 30%.
- The foil incidence needs to be limited to prevent detrimental cavitation effects. This limitation was not considered in the frequency domain method used to predict the T-foil effects in advance.
- The interaction between the T-foils and the hull was not considered. Interaction effects may be both favorable and unfavorable, depending on the frequency of motion. This will be elaborated in the following.

First, the forward foil wake sheet affects the flow at the aft foil. In steady flow the aft foil experiences a downwash over most of its span which reduces lift and increases induced drag. In waves, the vortex strength of the forward foil wake sheet will vary in time and in space. The aft foil lift force and its phase relative to the motion of the ship will be modified continuously. Figure 12 shows these effects on the foil pitch damping moment.



□ L_i, forward-aft foil interaction factor
Δ M_i, forward foil-hull interaction factor
∇ T_i, total interaction factor

Fig. 12 Interaction factors versus frequency of oscillation.

In the simulations, the foil system was subject to forced pitch oscillations whereby the forward foil wake sheet was a flat surface. The interaction factor L_i is defined as:

$$L_i = \frac{\left|M_f + M_a\right|_i}{\left|M_f + M_a\right|_0} \tag{26}$$

where M_f and M_a denote the pitch damping moment amplitudes due to forward and aft foil respectively and the subscripts i and 0 denote with and without interaction taken into account respectively. L_i shows an almost constant value of at low frequencies while at intermediate frequencies values above unity are attained while at high frequencies again a reduction in pitch moment occurs. The wake wave length, corresponding to the frequency where the interaction is most favourable, is twice the foil spacing, i.e. the downwash from the forward foil enhances the negative lift of the aft foil and vice versa for the upwash.

Second, mutual foil-hull interaction is caused by flow disturbances due to the hull at the T-foil position and by flow disturbances at the hull due to the T-foil vortex system. Calculations with and without hull and T-foils have shown that by far the largest interaction effect is due to the trailing vortex system of the forward T-foil. This vortex system runs below almost the entire submerged hull bottom. It induces there relatively small velocity components which in turn

result in small pressure differences. However, since the hull bottom area is large, the resulting vertical force is significant, in the order of 30% of the forward foil lift. Either a favorable or unfavorable interaction pitch moment is generated, depending on the encounter frequency. This is illustrated in Figure 12 where the factor M_i shows the ratio between the total pitch damping moment due to the hull and foils with and without taking interaction into account. M_i is defined as:

$$M_i = \frac{\left|M_h + M_f + M_a\right|_i}{\left|M_h\right|_0 + \left|M_f + M_a\right|_i} \qquad (27)$$

where M_h is the pitch damping moment amplitude acting on the hull. M_i values have been obtained by forced pitch oscillations with active foils. The factor M_i shows a similar behavior as L_i but with a sharper decrease in the high frequency region.

Finally, Figure 12 also shows the total interaction factor T_i which reflects the combination of L_i and M_i. For the TMV114 the wave encounter frequency showing the maximum pitch response is at 1.50 rad/sec, where the interaction is favorable. On the other hand, the peak frequency in the experimental wave spectrum corresponds to 2.0 rad/sec where the interaction effects are rather unfavorable. It is noted that for an improved T-foil control strategy, it might be worth while to account for the phase shifts in the pitching moment introduced by interaction.

High speed catamaran

Figure 13 shows a demi-hull of a slender, high speed catamaran hull form. Initial computations showed that interaction between the demi-hulls was negligible, which is not surprising in view of the high Froude number, F_{nL}=0.93, and the demi-hull spacing (y/L=0.26). Therefore, the motion response was determined for one demi-hull only. Since the buoyancy box is positioned relatively close to the undisturbed water surface, the hydrostatic forces on the instantaneous submerged body were taken into account. During the experiments the craft was equipped with an active trim tab to enhance pitch damping. The effects of the trim tab have been taken into account in the computations by using empirical data from a systematic series of model tests.

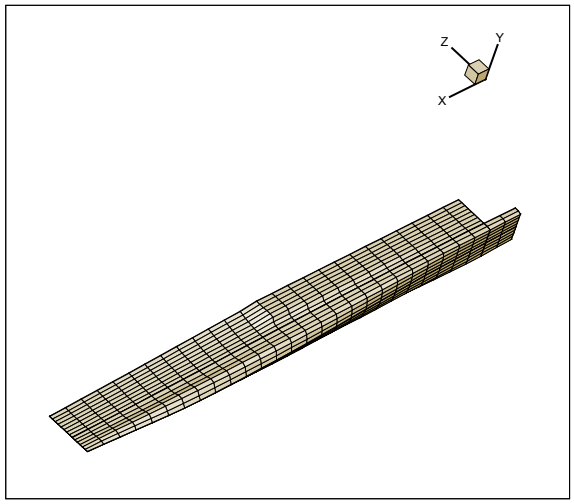
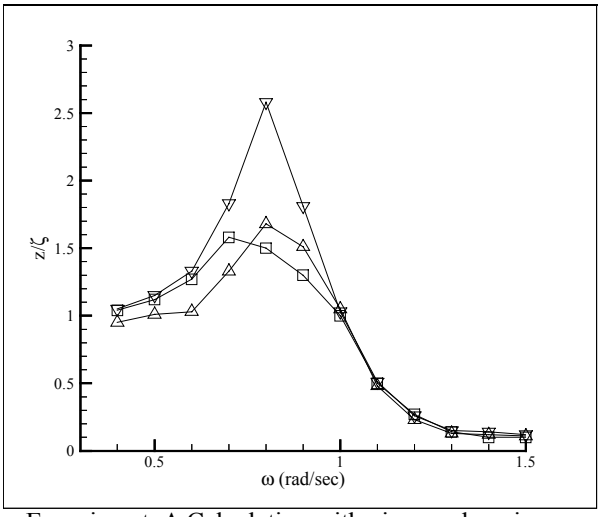


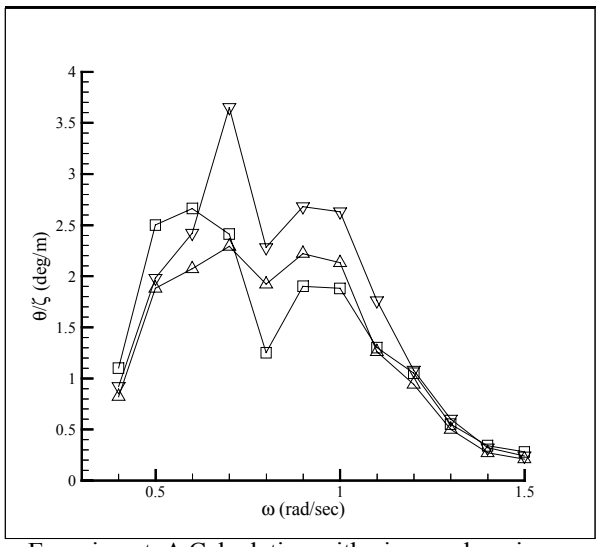
Fig. 13 Paneling arrangement on a demi-hull.

Figures 14 through 16 show the heave, pitch and forward vertical acceleration (at x/L=0.75) versus wave frequency. Experimental response functions are based on tests in irregular waves (H_s/L=0.026). Computed results (regular waves) are given with and without viscous damping in the vertical plane. It is clear that adding viscous damping is necessary for an adequate prediction of the peak responses. Despite the fact that the computed pitch response deviates from the experimental response at the peak frequency, the vertical accelerations are in reasonably good agreement.



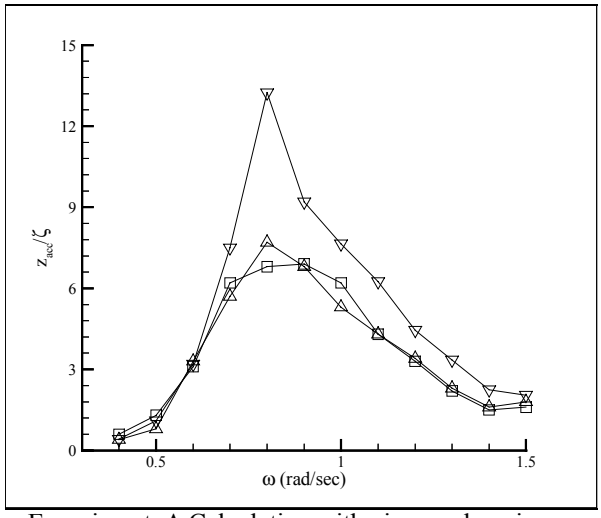
□ Experiment Δ Calculation with viscous damping
∇ Calculation without viscous damping

Fig. 14 Heave response of catamaran in head waves at F_{nL} =0.93.



□ Experiment Δ Calculation with viscous damping
∇ Calculation without viscous damping

Fig. 15 Pitch response of catamaran in head waves at F_{nL} =0.93.



□ Experiment Δ Calculation with viscous damping
∇ Calculation without viscous damping

Fig. 16 Vertical acceleration response of catamaran in head waves at F_{nL} =0.93.

Conceptual frigate hull form

The last case concerns a conceptual hull form that was developed during a study into advanced future mono hull concepts for the Royal Netherlands Navy. This so-called Cofea (Coefficient Of Floatation Extremely Aft) hull form intended, and proved, to have relatively low vertical accelerations at the ship ends. The hull form is rather unusual and presents a good validation case. Figure 17 shows the paneling arrangement. The fore body is Swath-like. The aft body is relatively wide at the water surface while its transom submergence is small. Experimental results show that the peak heave and pitch responses are strongly non-linear, therefore besides linear also some non-linear computational results are shown. Computing accurate Green function contributions for aft body panels close to the transom proved to be difficult. It was necessary to maintain a minimum panel submergence of 50% of the panel width for transom and waterline panels. Figures 18 and 19 show linear and experimental heave and pitch responses. The linear results correspond to tests in low regular waves (H/L=0.017) and are close to the experimental results. At the peak frequency a non-linear result is given (H/L=0.025). The reduction in heave and pitch response is well predicted for pitch but deviates somewhat for heave.

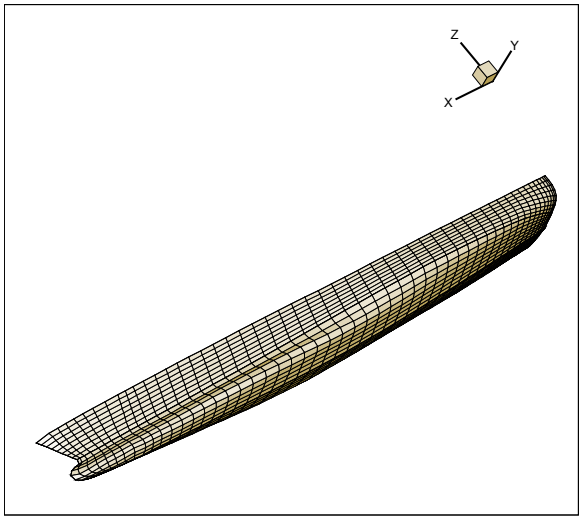


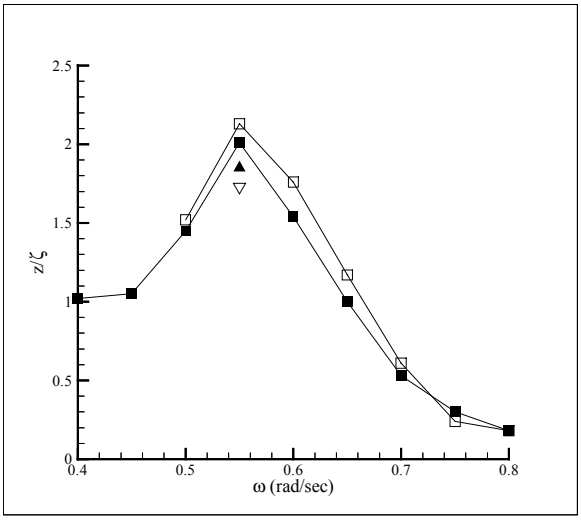
Fig. 17 Paneling arrangement on Cofea frigate

CONCLUDING REMARKS

A time domain panel method is presented for motion prediction of ships with (and without) ride control systems. The method is applied to a number of practical cases for which experimental results are available.

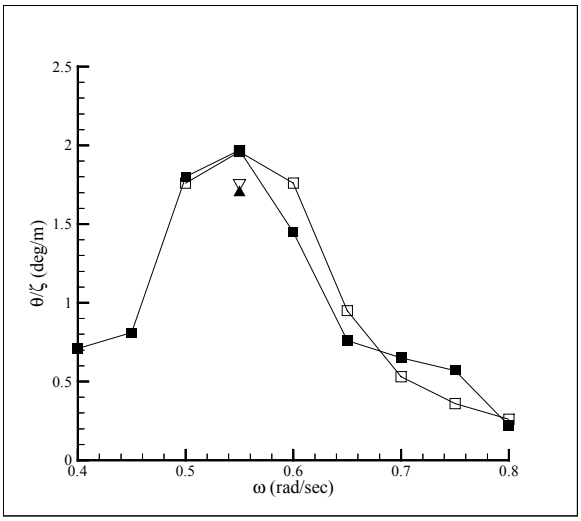
Computed results for damping and wave excitations forces on a lifting surface advancing below a free surface are in fair agreement with experimental data.

Next the heave and pitch motions for a destroyer hull form sailing in head waves are adequately predicted.



□ Experiment $H/L = 0.017$
■ Calculation $H/L = 0.017$
Δ Experiment $H/L = 0.025$
▲ Calculation $H/L = 0.025$

Fig. 18 Heave response of Cofea in head waves



□ Experiment $H/L = 0.017$
■ Calculation $H/L = 0.017$
Δ Experiment $H/L = 0.025$
▲ Calculation $H/L = 0.025$

Fig. 19 Pitch response of Cofea in head waves

For a high speed mono hull ferry the effect of interaction between a set of T-foils and the T-foils and the hull is studied. Interaction is shown to be significant and may have a favorable as well as an unfavorable effect on the pitch damping efficiency of the T-foils. The importance of a transom stern modeling is shown as well for this case.

For a high speed catamaran the need to include viscous damping is shown. Heave and pitch motions in head waves are in reasonably good agreement with experimental data. Accelerations are well predicted.

For a conceptual frigate hull form heave and pitch responses in low waves are well predicted by the linear seakeeping method. In higher waves, non-linear effects are reasonably well predicted at the frequency where the peak responses occur.

It is concluded that the linear computational method is well suited for analyzing the motion responses of (fast) ships in head waves, with and without utilizing ride control systems.

Future developments include a more accurate evaluation of the free surface Green function for shallowly submerged panels by using a combination of analytical and numerical integration and the inclusion of viscous damping for roll, sway and yaw motions.

ACKNOWLEDGEMENTS
The author gratefully acknowledges the permission of Rodriquez Engineering SrL. for permission to use the experimental data of the TMV114 design and the permission of the Royal Netherlands Navy to show the experimental data of the Cofea concept.

REFERENCES

Katz J. and Plotkin A., "Low Speed Aerodynamics – From Wing theory to Panel Methods", Mc Graw-Hill Inc., New York.

Kyozuka Y., "The Unsteady lift on a Two-Dimensional Wing Oscillating below a Free Surface", Proceedings of the Second International Offshore and Polar Engineering Conference, San Francisco, USA, 1992.

Lin W.M. and Yue D., "Numerical Solutions for Large-Amplitude Ship Motions in the Time Domain", Proceedings of the 18th Symposium on Naval Hydrodynamics, Ann Arbor, 1990, pp 41-65.

Newman J.N., "The Evaluation of Free Surface Green Functions", Fourth International Symposium on Numerical Ship Hydrodynamics, Washington, USA, 1985, pp 4-19.

Newman J.N., "The Approximation of Free Surface Green Functions", In: P.A. Martin and G.R. Wickham, Editors, Wave Asymptotics, Cambridge University Press, 1992, pp 107-135.

Pieters M.J.A., "On the differential properties of the time domain Green function of linearized free-surface hydrodynamics", Master Thesis, Delft University of Technology, Department of Mathematical Physics, 1999.

Pinkster H.J.M., "Three dimensional time-domain analysis of fin stabilised ships in waves", Graduation Report, Delft University of Technology, Department of Applied Mathematics, 1998.

Walree F. van, "Computational Methods for Hydrofoil Craft in Steady and Unsteady Flow", Ph.D. Thesis, Delft University of Technology, Department of Naval Architecture and Marine Engineering, March 1999.

Wilson M.B., "Experimental Determination of Low Froude Number Hydrofoil Performance in Calm Water and in Regular Waves", Proceedings of the 20th American Towing Tank Conference, Hoboken, New Jersey, USA, 1983.

DISCUSSION

Robert Beck
University of Michigan, USA

How did you include the viscous convections in your computations?

AUTHOR'S REPLY

The viscous corrections were included by using a strip theory like approach. For each strip in-between two adjacent sections the local relative fluid velocity was determined. Together with a constant viscous drag coefficient and a reference area (sectional width times length) the viscous force is determined.

DISCUSSION

Woei-Min Lin
Science Applications International Corporation, USA

I would like to learn from Dr. Walree how the ventilated transom stern model was implemented. How was the geometry of the dummy body behind the transom determined? Did the dummy body shape depend on what type of hydrodynamic problem (e.g. forward speed only, forward speed with heave and pitch motion, etc.) was solved?

AUTHOR'S REPLY

The geometry of the dummy body behind the transom is a linear backwards extrapolation of the transom section and the first section in front of the transom. The shape of the dummy body did not depend on the hydrodynamic problem. The dummy body approach is a simple way to force the flow to leave the transom edge parallel to the hull buttocks and without unrealistic velocity magnitudes.

DISCUSSION

S.R. Turnock
University of Southampton, United Kingdom

The interaction between the forward foil wake and hull and rear foil is important. Could the author comment on the validity of a fixed position wake for the time domain case where circulation varies through zero. Is there experimental evidence to show how the forward wake tracks and breaks up behind the vessel?

AUTHOR'S REPLY

The interaction between the forward foil wake and hull and rear foil is important indeed. A fixed position wake is consistent with the assumptions of a linearized method and is computationally cheap. It is possible to approximate the real wake sheet shape in a non-linear method, including wake sheet roll-up, but at a substantial computational burden. Experimental results on the interaction between two tandem foils running in head waves show that a fixed position forward foil wake is allowed for small to moderate heave and pitch motions. Moderate motions in this respect are typically one half of the foil submergence below the free surface. For motions in the horizontal plane no information on this matter is available.

Furthermore, comparing linear and non-linear computational results shows that there may exist a substantial effect of the actual wake sheet shape on forward-aft foil interaction, i.e. the aft foil lift, if the combination of foil spacing and oscillation frequency is such that the aft foil continuously operates in or close to the forward foil wake sheet.

To the authors' knowledge there is little experimental information on the track and break down of wake sheets below a free surface. In an unbounded domain, a lot of information is available from the aeronautical field.